I. SUPPLEMENTARY THEORY

A. Viscoelastic case

The assumption that the tissue shell is a linearly elastic material is simple and convenient, but false. A more general constitutive law for a multi-cellular tissue cell would have to account for both its viscous and plastic behavior when deformation is followed by self-adaptation via cell rearrangement [2, 3]. In the main text we presented a elastic-plastic regime as a minimum model to reproduce the nonlinearities observed in the experiment, however, in the general case we should expect a visco-elastic or even visco-plastic regime.

Here, we briefly discuss the role of viscoelastic deformations by using

$$\dot{\sigma} + \frac{\sigma}{\tau} = \frac{E}{R}\frac{dR}{dt} \tag{S1}$$

instead of the purely elastic or elastic-plastic model used in the main text. Here $\tau = \eta_{\rm cyst}/E$, being E the elastic modulus, and $\eta_{\rm cyst}$ the viscosity of the shell. Then, the system of differential equations (6-8) in the main text are replaced by:

$$\frac{d\hat{R}}{d\hat{t}} = (1 - \hat{P}/\hat{P}_{\rm osm} - Q/J_{\rm o}) \equiv \hat{\Phi} \tag{S2}$$

$$\frac{d\hat{h}}{d\hat{t}} = \frac{J_c}{4\pi R_0^2 J_{\rm o}}\frac{1}{\hat{R}^2} - \frac{2\hat{h}}{\hat{R}}\hat{\Phi} \tag{S3}$$

$$\frac{d\hat{P}}{d\hat{t}} = \frac{1}{\hat{R}^2}\left((2\hat{h} - 3\hat{P}\hat{R})\hat{\Phi} + \frac{J_c}{4\pi R_0^2 J_o}\frac{\hat{P}}{\hat{h}}\right) - \frac{\hat{P}R_0}{\tau J_o} \tag{S4}$$

In the viscoelastic case, there is one extra dimensionless parameter accounting for the ratio between the timescales for cyst expansion and viscoelastic deformation $R_0 E/\eta_{\rm cyst} J_{\rm o}$. The additional parameter allows for the explanation of the average radius increase observed in the experiments with synthetic cysts. However, the values of the viscoelastic coefficient needed to reproduce the experimental behavior are too high to correspond to biological tissue, which has a viscosity around $10^2 {\rm kPa}\cdot s$ [4] (Fig. S7)

B. Pore dynamics

The pore opening and closing can be represented in terms of a simple dynamical system :

$$\frac{dr}{dt} = a_1 r + a_2 r^3 - a_3 r^5 \tag{S5}$$

$$a_1 = \frac{\sigma - \sigma_2}{4(\sigma_2 - \sigma_1)} \frac{1}{\tau_{\text{pore}}} \tag{S6}$$

$$a_2 = \frac{1}{\tau_{\text{pore}} b_0^2} \tag{S7}$$

$$a_3 = \frac{1}{\tau_{\text{pore}} b_0^4} \tag{S8}$$

the normal form for a subcritical pitchfork bifurcation where the maximum pore size is b_0 and the characteristic time for healing is τ_{pore}. When the dynamics of the pore are much faster than the capsule dynamics, $\tau_{\text{pore}} << \tau_{\text{growth}}$, the dynamics can be approximated by a step function, in that case the pore has only two possible states and the transition between them occurs instantaneously, $r = b_0$ after it opens at $\sigma = \sigma_2$, and $r = 0$ after closing at $\sigma = \sigma_1$ (Fig.S3). If $\tau_{\text{pore}} \sim \tau_{\text{growth}}$, the pore does not heal instantaneously, and the amplitude of the oscillations varies as a function of τ_{pore}. We found that slow pore dynamics increases the amplitude and the period of oscillations while keeping the maximum radius constant (Fig.S6). This happens because although bursting occurs at the same radius for all rates of pore closing, when healing times are slower, the pore closes at smaller values of the tension, which allows more fluid to enter the cyst.

It should be pointed out that our minimal mathematical model for hole opening above a critical tissue tension has some similarities with pore opening and closing in lipid vesicles and membranes [5, 6]. However, the length and time-scales are orders of magnitude apart, and the rheology and regulatory mechanisms are very different.

II. MOVIES

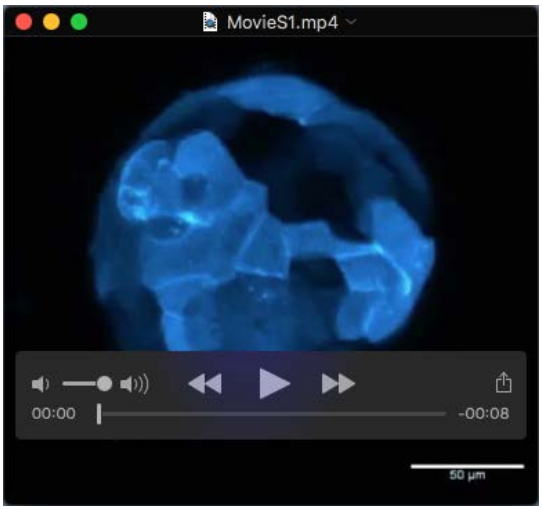

Movie 1. Confocal live imaging of an encapsulated cyst grown from cells stably transfected with LifeAct-GFP. Maximum intensity projections of the confocal stacks [a hot look-up table acquired using Fiji is shown (cyan)]. Total duration=19h

Movie 2. Growth of an MCF10DCIS.com cyst inside an alginate gel capsule. Time-lapse, phase-contrast imaging shows the oscillations of the cyst before reaching the walls of the capsule. Images were recorded every 5 min. Scale bar: 100μm.

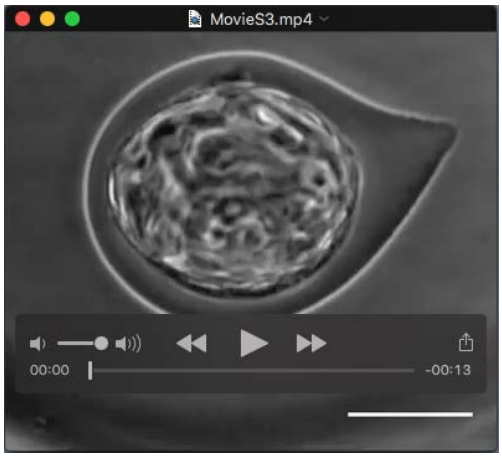

Movie 3. Growth of an MCF10DCIS.com cyst inside an alginate gel capsule. Time-lapse, phase-contrast imaging shows the oscillations of the cyst in contact with the capsule inner wall. Images were recorded every 5 min. Scale bar: 100μm.

Movie 4. Growth of an MCF10DCIS.com cyst inside an alginate gel capsule. Time-lapse, phase-contrast imaging shows the oscillations of the cyst in contact with the capsule inner wall, bursting of the capsule, escape of the cyst, which then undergoes inflation-deflation cycles outside the capsule. Images were recorded every 5 min. Scale bar: 100μm.

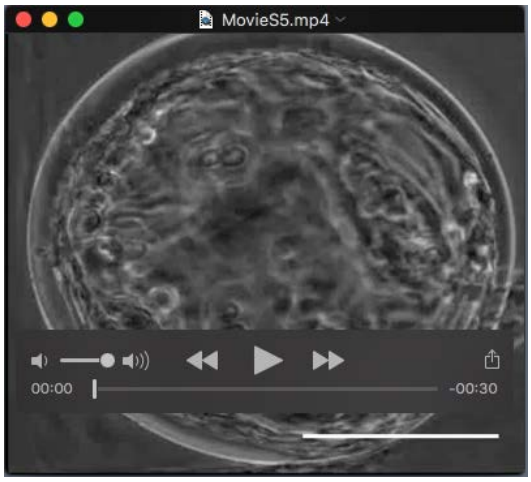

Movie 5. Phase contrast sequence showing the collapse of a cyst. Images were recorded every 5 s. Scale bar: 100μm.

Movie 6. Phase contrast sequence of a punching experiment. An encapsulated cyst is maintained using micropipette aspiration and punched with a glass needle Images were recorded every 1 s. Scale bar: 100μm.

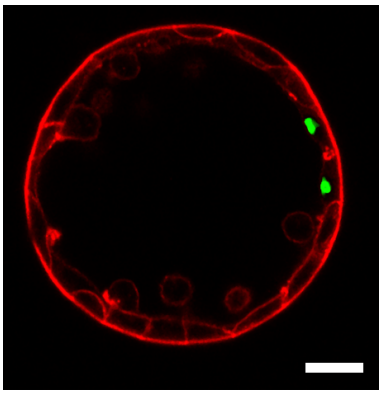

Figure S1. Confocal image of the equatorial plane of a cyst stained with for actin (red) and apoptosis (green). Scale bar: 50μm.

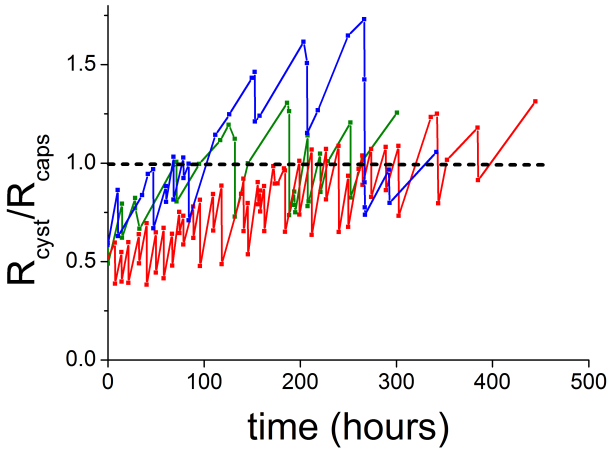

Figure S2. Representative trajectories of cyst radius for cysts with different sizes. Radius is normalized by the inner radius of the capsule.

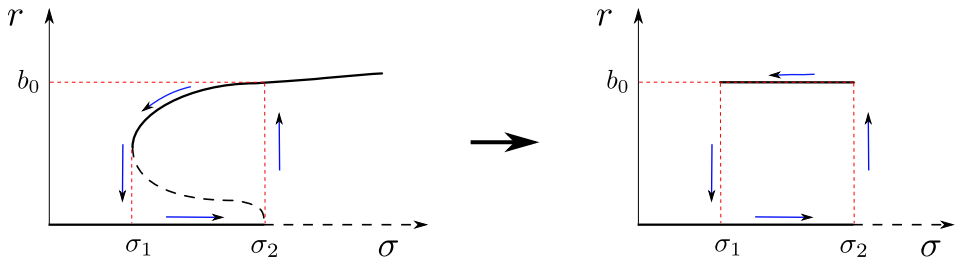

Figure S3. Subcritical pitchfork bifurcation approximated as a step function assuming that pore dynamics is much faster than growth with threshold tension for rupture (σ_2) and healing (σ_1) and pore size b_0.

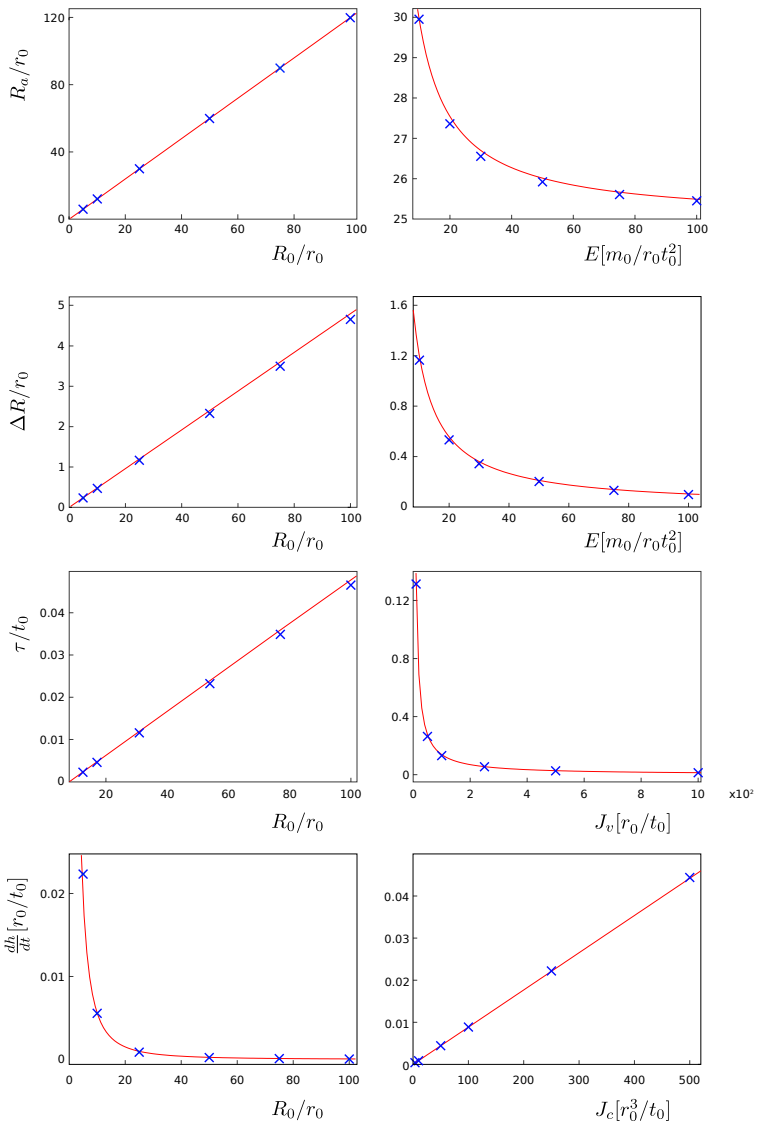

Figure S4. Comparison between theoretical estimates (line) and numerical results (cross) in the limit of small strains.

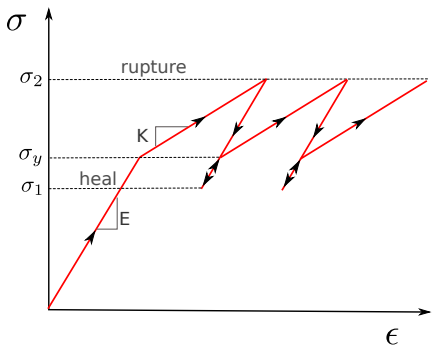

Figure S5. Schematic of the strain-stress relation for consecutive cycles for a linear elastic-plastic material with a threshold tension for rupture (σ_2) and healing (σ_1) and yield tension σ_y.

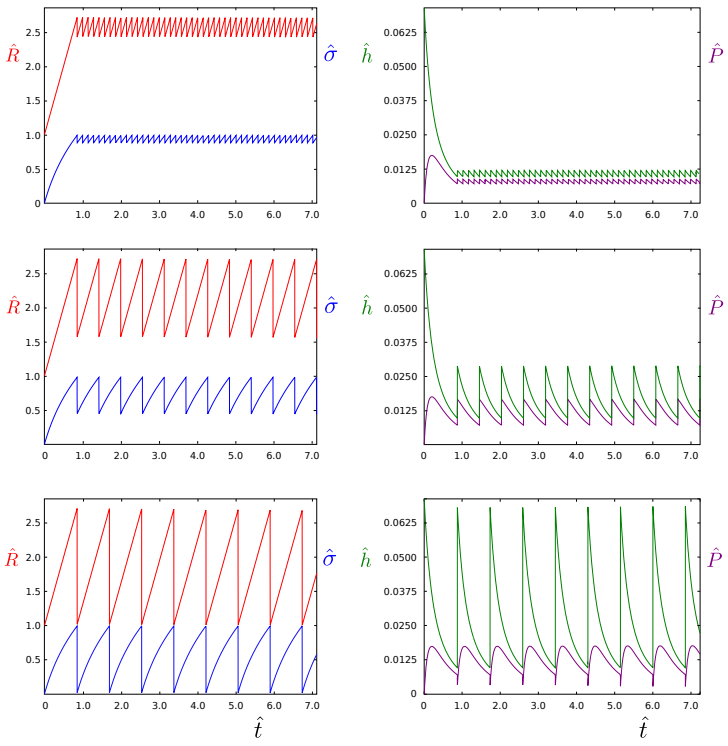

Figure S6. System dynamics for different pore closing times $\hat{\tau}_{\text{pore}} = \tau_{\text{pore}}/\tau_{\text{growth}}$. From top to bottom: $\hat{\tau}_{\text{pore}} = 5.7 \cdot 10^{-7}$, $\hat{\tau}_{\text{pore}} = 7.1 \cdot 10^{-6}$, $\hat{\tau}_{\text{pore}} = 2.9 \cdot 10^{-5}$. The rest of the dimensionless parameters are $\hat{j} = 0.008$, $e = 4.6 \cdot 10^{11}$, $\hat{\sigma}_2 = 1$, $\hat{h}_0 = 0.07$, $\hat{b}_0 = 0.036$, $\Delta\hat{\sigma} = 0.2$, $\hat{\sigma}_0 = \hat{P}_0 = 0$.

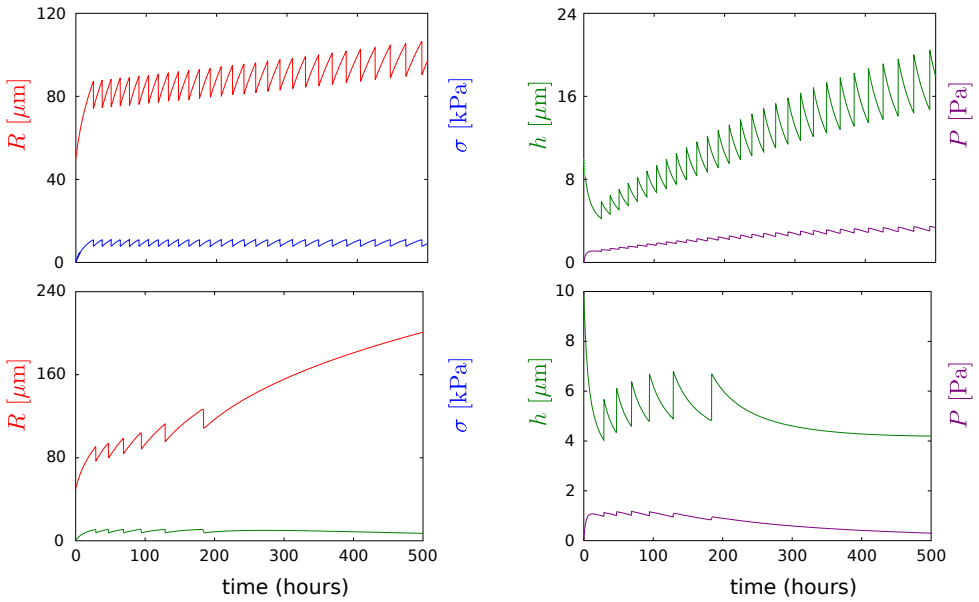

Figure S7. System trajectories for the viscoelastic case for $J_o = 25\mu m^3/s$, $J_c = 1\mu m^3/s$, $E = 20$kPa, $\sigma_2 = 11$kPa, $R_0 = 50\mu m$, $h_0 = 10\mu m$ and viscous coefficient (top) $\eta = 7.9 \cdot 10^7 \text{kPa} \cdot s$ and (bottom) $\eta = 1.6 \cdot 10^7 \text{kPa} \cdot s$

[1] Alessandri, K., Sarangi, B. R., Gurchenkov, V. V., Sinha, B., Kieß ling, T. R., Fetler, L., Rico, F., Scheuring, S., Lamaze, C., Simon, A., Geraldo, S., Vignjevic, D., Doméjean, H., Rolland, L., Funfak, A., Bibette, J., Bremond, N., and Nassoy, P. (2013).

[2] D. Gonzalez-Rodriguez, K. Guevorkian, S. Douezan, and F. Brochard-Wyart, "Soft matter models of developing tissues and tumors.," Science (New York, N.Y.), vol. 338, pp. 910–7, Nov. 2012.

[3] L. Preziosi, D. Ambrosi, and C. Verdier, "An elasto-visco-plastic model of cell aggregates.," Journal of theoretical biology, vol. 262, pp. 35–47, Jan. 2010.

[4] J. J. Muñoz and S. Albo, "Physiology-based model of cell viscoelasticity," Physical Review E, vol. 88, p. 012708, July 2013.

[5] Koslov, M. and Markin, V. (1984). A theory of osmotic lysis of lipid vesicles. J. Theor. Biol., 109(1):17–39.

[6] Evans, E. and Heinrich, V. (2003). Dynamic strength of fluid membranes. Comptes Rendus Phys., 4(2):265–274.